Differences in the critical dynamics underlying the human and fruit-fly connectome

Géza Ódor,[1] Gustavo Deco,[2] and Jeffrey Kelling[3]

[1]*Institute of Technical Physics and Materials Science, Center for Energy Research, P. O. Box 49, H-1525 Budapest, Hungary*

[2]*Center for Brain and Cognition, Theoretical and Computational Group, Universitat Pompeu Fabra / ICREA, Barcelona, Spain*

[3]*Department of Information Services and Computing, Helmholtz-Zentrum Dresden - Rossendorf, P.O.Box 51 01 19, 01314 Dresden, Germany*

(Received 28 November 2021; accepted 7 March 2022; published 20 April 2022)

Previous simulation studies on human connectomes suggested that critical dynamics emerge subcritically in the so-called Griffiths phases. Now we investigate this on the largest available brain network, the 21662 node fruit-fly connectome, using the Kuramoto synchronization model. As this graph is less heterogeneous, lacking modular structure and exhibiting high topological dimension, we expect a difference from the previous results. Indeed, the synchronization transition is mean-field-like, and the width of the transition region is larger than in random graphs, but much smaller than as for the KKI-18 human connectome. This demonstrates the effect of modular structure and dimension on the dynamics, providing a basis for better understanding the complex critical dynamics of humans.

DOI: 10.1103/PhysRevResearch.4.023057

I. INTRODUCTION

Power-law (PL)-distributed neuronal avalanches were shown in neuronal recordings [spiking activity and local field potentials (LFPs)] of neural cultures *in vitro* [1–4], LFP signals *in vivo* [5], field potentials and functional magnetic resonance imaging (fMRI) blood-oxygen-level-dependent (BOLD) signals *in vivo* [6,7], voltage imaging *in vivo* [8], and 10–100 single-unit or multiunit spiking and calcium-imaging activity *in vivo* [9–12]. Furthermore, source reconstructed magneto- and electroencephalographic recordings (MEG and EEG), characterizing the dynamics of ongoing cortical activity, have also shown robust PL scaling in neuronal long-range temporal correlations. These are at time scales from seconds to hundreds of seconds and describe behavioral scaling laws consistent with concurrent neuronal avalanches [13]. However, the measured scaling exponents do not seem to be universal. Besides the experiments' theoretical research provide evidence that the brain operates in a critical state between sustained activity and an inactive phase [14–25].

Criticality in general occurs at continuous, second-order phase transitions and a ubiquitous phenomenon in nature as systems can benefit many ways from it. As correlations and fluctuations diverge [26] in neural systems working memory and long-range interactions can be generated spontaneously [27] and the sensitivity to external signals is maximal. Furthermore, it has also been shown that information-processing capabilities are optimal near the critical point. Therefore, systems tune themselves close to criticality via self-organization (SOC) [28,29], presumably slightly below to avoid blowing over excitation. However, criticality is not a necessary condition for power-law statistics to appear, see Ref. [30], so the presented numerical results do not provide a full proof for the criticality hypothesis of the whole brain, but remain within the validity of model assumptions.

Besides, if quenched heterogeneity (that is called disorder compared to homogeneous system) is present, rare-region (RR) effects [31] and an extended semicritical region, known as Griffiths phase (GP) [32] can emerge. RRs are very slowly relaxing domains, remaining in the opposite phase than the whole system for a long time, causing slow evolution of the order parameter. In the entire GP, which is an extended control parameter region around the critical point, susceptibility diverges and autocorrelations exhibit fat-tailed, power-law behavior, resulting in bursty behavior [33], frequently observed in nature [34]. Even in infinite-dimensional systems, where mean-field behavior is expected, Griffiths effects can occur in finite time windows [35].

Heterogeneity effects are very common in nature and result in dynamical criticality in extended GPs, in case of quasistatic quenched disorder approximation [36]. This leads to avalanche size and time distributions, with nonuniversal power-law tails. It has been shown within the framework of modular networks [36–38] and a large human connectome graph [39,40,41]. The word "connectome" is defined as the structural network of neural connections in the brain [42]. Recently the hemibrain has been derived from a three-dimensional (3D) image of roughly half the fruit-fly (FF) brain. It contains verified connectivity between 25000 neurons that form more than 20×10^6 connections [43,44]. However, as this is not a complete central nervous system many of the connections do not connect to the nodes published.

As individual neurons *in vitro* emit periodic signals [45], it is tempting to use oscillator models and to investigate criticality at the synchronization transition point. Note, however that

according to other experiments they can also show a variety of spiking behaviors. Recently, a brain model analysis using Ginzburg-Landau-type equations concluded that empirically reported scale-invariant avalanches can possibly arise if the cortex is operated at the edge of a synchronization phase transition, where neuronal avalanches and incipient oscillations coexist [46].

One of the most fundamental models showing phase synchronization is the Kuramoto model of interacting oscillators [47] and was used to study synchronization transition on various synthetic and connectome graphs available [48–52]. Note, that the Kuramoto equation, while neglecting the integration feature of spiking activity of neighboring neurons, still provides a fundamental, mechanistic model for synchronization transition and criticality. It also involves the quasistatic assumption, according to which the time scale of network change is much larger than the time scale of reaching the steady state of the processes running on it. That means it is permissible to focus on determining the critical dynamics on a snapshot of the connectome, not taking plasticity and learning into account. There is also uncertainty in the KKI-18 full human brain connectome structure as discussed in Ref. [41], but a recent study claims that diffusion tensor imaging is in good agreement with ground-truth data from histological tract tracing [53].

Because of quenched, purely topological heterogeneity an intermediate phase was found between the standard synchronous and asynchronous phases, showing frustrated synchronization, metastability, and chimeralike states [54]. This complex phase was investigated further in the presence of noise [49] and on a simplicial complex model of manifolds with finite and tunable spectral dimension [50] as a simple model for the brain.

In case of a representative of large human white matter connectomes [39] the $N = 804\,092$ node KKI-18 network GPs have been found via measuring the desynchronization times of local perturbations [51,52]. Now we extend this kind of investigation via Kuramoto model (KM) on the FF connectome. The comparison of the synchronization transition results on the KKI-18 and FF is valid, because for FF we know the full topology of the neural network and for KKI-18 the unknown, microscopic details below its 1 mm^3 resolution are not expected to affect the long-wavelength behavior determining the critical properties. Our model describes a resting state brain. External sources, leading to the well-known Widom line phenomena have recently been studied both by experiments and simulations. Quasicriticality, generated by external excitation, was suggested to explain the lack of universality observed in different experiments [55].

II. TOPOLOGY OF THE FRUIT-FLY CONNECTOME

We downloaded the hemibrain data set (v1.0.1) from Ref. [56]. It has $N_{FF} = 21662$ nodes and $L_{FF} = 3\,413\,160$ edges, out of which the largest single connected component contains $N = 21615$ and $L = 3\,410\,247$ directed and weighted edges, that we used in the simulations. The number of incoming edges varies between 1 and 2708. The weights are integer numbers, varying between 1 and 4299. The average node degree is $\langle k \rangle = 315129$ (for the in-degrees it is: 1576),

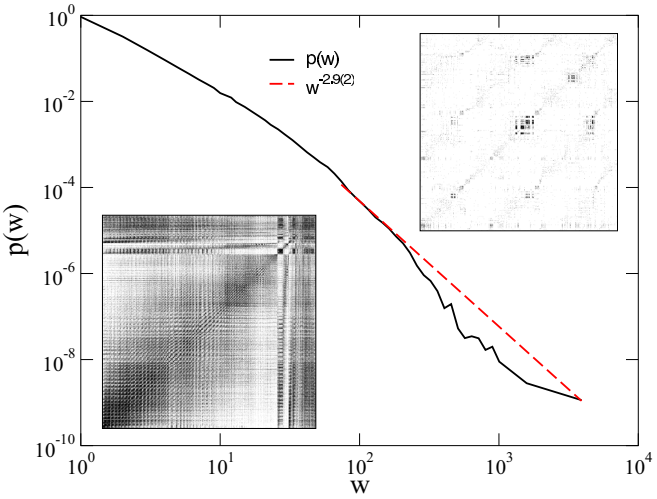

FIG. 1. Weight distribution of the fruit-fly connectome. Right inset: adjacency matrix plot of the fruit-fly connectome. Left inset: full adjacency matrix down sampled with a max pooling kernel of size 10×10. Black dots denote connections between presynaptic and postsynaptic neurons. Right inset: zoom-in to the center of the matrix without down sampling.

while the average weighted degree is $\langle w \rangle = 628$. The adjacency matrix is visualized by the insets of Fig. 1. One can see a rather homogeneous, almost structureless network, however, it is not random, as discussed in the graph analysis [57]. For example, the degree distribution is much wider than that of a random Erdős-Rényi (ER) graph and exhibits a fat tail.

The weight distribution $p(w)$ we obtained by exponentially growing bin sizes: $w_i \propto 1.12^i$ can can be seen on Fig. 1. Interestingly, the tail of $p(w)$ shows a nontrivial shape, as compared to Fig. 5 of Ref. [57], where this fine structure cannot be seen, due to the linear binning used there. A fitting for the whole weight distribution data, assuming a PL with exponential cutoff is published in Ref. [57], which is characterized by the exponent -1.67. The application of growing bin sizes on the weights of the available traced connections does not suggest an exponential cutoff, but a PL tail with an exponent $-2.9(2)$ could be fitted for the $w > 100$ region. We think this might be relevant, because in case of KKI-18 connectome a similar PL was found for the tail of link weight distribution and maybe it is related to an optimal weight distribution (counting the multiplicity of edges) in real networks embedded in the 3D space. Of course, due to the partial FF connectome data, we assume that the additional, omitted edges result in a tail with a finite exponential size cutoff.

The modularity quotient of the FF network defined by

$$Q = \frac{1}{N\langle k \rangle} \sum_{ij} \left(A_{ij} - \frac{k_i k_j}{N\langle k \rangle} \right) \delta(g_i, g_j), \tag{1}$$

is very low: $Q = 0.002264$, where A_{ij} is the adjacency matrix and $\delta(i, j)$ is the Kronecker delta function. The weighted modularity quotient is even lower: $Q_w = 0.0001184$. In comparison, the modularity quotient of the KKI-18 network is about 40 times greater: $Q_w = 0.0047$.

The Watts-Strogatz clustering coefficient [58] of a network of N nodes is

$$C = \frac{1}{N}\sum_i 2n_i/[k_i(k_i-1)], \tag{2}$$

where n_i denotes the number of direct edges interconnecting the k_i nearest neighbors of node i. This is $C_{FF} = 0.191$, about 12.36 times larger than that of a random network of same size: $C_r = 0.01545$, obtained by $C_r = \langle k\rangle/N$. In case of KKI-18 we found: $C_{KKI-18} = 0.5$.

The average shortest path length is defined as

$$L = \frac{1}{N(N-1)}\sum_{j\neq i} d(i,j), \tag{3}$$

where $d(i, j)$ is the graph distance between vertices i and j. For FF this is $L_{FF} = 2.7531$, about 1.3 times larger than that of the random network of same size: $L_r = 2.1162$, following from the formula [59]:

$$L_r = \frac{\ln(N) - 0.5772}{\ln\langle k\rangle} + 1/2. \tag{4}$$

So, the FF is a small-world network, according to the definition of the coefficient [60]:

$$\sigma = \frac{C/C_r}{L/L_r}, \tag{5}$$

because $\sigma_{FF} = 9.5$ is much larger than unity.

We estimated the effective graph (topological) dimension, which is obtained by the breadth-first search algorithm: $d = 5.4(5)$, which is defined by $N(r) \sim r^d$, where we counted the number of nodes $N(r)$ with chemical distance r or less from the seeds and calculated averages over the trials. Note, however that finite-size cutoff happens already for $r > 2$. This dimension renders this model into the mean-field region, because the upper-critical dimension is $d_c = 4$.

III. NUMERICAL ANALYSIS OF THE KURAMOTO MODEL

We used the KM of interacting oscillators [47] to study the synchronization on the human KKI-18, the FF connectome as well as on ER random graphs for comparison KM was originally defined on full graphs, corresponding to mean-field behavior [61]. The critical dynamical behavior has recently been explored on various random graphs [51,62,63]. Phase transition in the KM can happen only above the lower critical dimension $d_c^- = 4$ [64]. In lower dimensions, a true, singular phase transition in the $N \to \infty$ limit is not possible, but partial synchronization can emerge with a smooth crossover if the oscillators are strongly coupled.

The KM describes interacting oscillators with phases $\theta_i(t)$ located at N nodes of a network, which evolve according to the dynamical equation

$$\dot{\theta}_i(t) = \omega_{i,0} + K\sum_j W_{ij}\sin[\theta_j(t) - \theta_i(t)]. \tag{6}$$

Here, W_{ij} is the weighted adjacency matrix and summation is performed over neighboring nodes of i. There is a quenched heterogeneity in W_{ij} as well as in $\omega_{i,0}$, which is the intrinsic frequency of the ith oscillator, drawn from a $g(\omega_{i,0})$ distribution. The global coupling K is the control parameter of the model by which we can tune the system between asynchronous and synchronous states. One usually follows the synchronization transition through studying the Kuramoto order parameter defined by

$$R(t) = \frac{1}{N}\left|\sum_{j=1}^{N} e^{i\theta_j(t)}\right|, \tag{7}$$

which is nonzero above a critical coupling strength $K > K_c$ or tends to zero for $K < K_c$ as $R \propto \sqrt{1/N}$. At K_c, R exhibits growth as

$$R(t, N) = N^{-1/2}\, t^{\eta}\, f_{\uparrow}(t/N^{\tilde{z}}), \tag{8}$$

with the dynamical exponents $\tilde{z}$ and η, if the initial state is incoherent.

Additionally, we have also calculated another order parameter, which measures the spread of frequencies

$$\Omega(t, N) = \frac{1}{N}\sum_{j=1}^{N}(\overline{\omega} - \omega_j)^2, \tag{9}$$

In case of a single peaked self-frequency distribution it is an appropriate order parameter, besides the more commonly used measure, which counts the number of oscillators in the largest cluster having an identical frequency [64].

Generally we used the Runge-Kutta-4 integration algorithm with step sizes $\delta = 0.01$ or $\delta = 0.1$ if it was sufficient, via a special, parallel algorithm, running on GPUs. We have averaged over the solutions for thousands of different initial self-frequencies, chosen randomly from Gaussian distributions with zero mean and unit variance at each control parameter value. In a previous paper [52], we have shown the possibility of rescaling these onto more realistic, narrow-banded frequencies thanks to the Galilean invariance of the KM. Some of the runs, especially for larger couplings $K \geqslant 3$, were tested by the adaptive solver Bulrisch-Stoer [65] of the boost library. For very large couplings, $K > 30$ only the adaptive solver could provide reasonable results.

First, we have determined the growth behavior of $R(t)$ of the Kuramoto equation solution with incoming weight normalization, in order to mimic a local homeostasis, provided by the unknown balance of inhibition/excitation:

$$W'_{ij} = W_{ij}/\sum_{j\,\in\,\text{neighb. of i}} W_{ij}. \tag{10}$$

This renormalization has been used in previous connectome studies [40,41,51,52,66]. Recently, a comparison of modeling and experiments arrived at a similar conclusion: equalized network sensitivity improves the predictive power of a model at criticality in agreement with the fMRI correlations [66]. The solution of equations was started from incoherent states, but for larger K values it was better to start from coherent states in order to reach the steady states without large oscillations.

As Fig. 2 shows there is a transient region up to $t < 30$ followed by a level off as the correlation length exceeds the system size, causing a steady-state saturation of the phase synchronization. In the transient region curves with $K > 1.7$ exhibit an upward curvature, while those with $K < 1.7$ exhibit

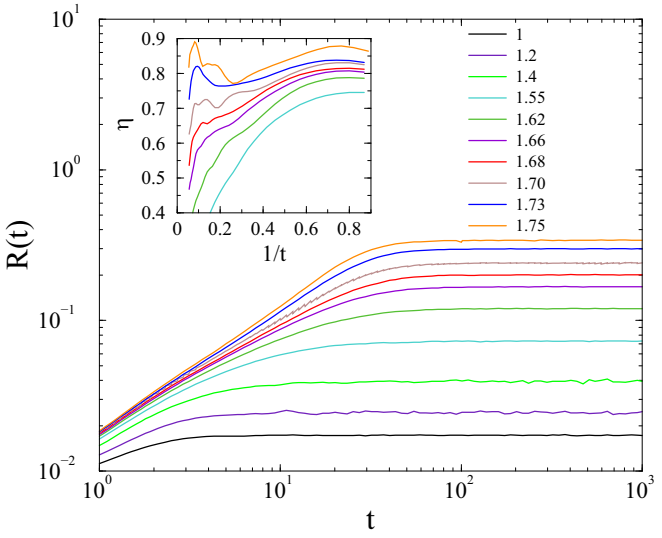

FIG. 2. Growth of $R(t)$ on the weight normalized FF, using incoherent initial state for different K global coupling values as shown by the legends. One can locate a transition by the convex/concave criterion at $K_c = 1.70(2)$, where an initial PL growth can be observed. The inset shows the local slopes of the same data on $1/t$ scale with the same color coding from $K = 1.75$ (top curve) to $K = 1.55$ (bottom curve).

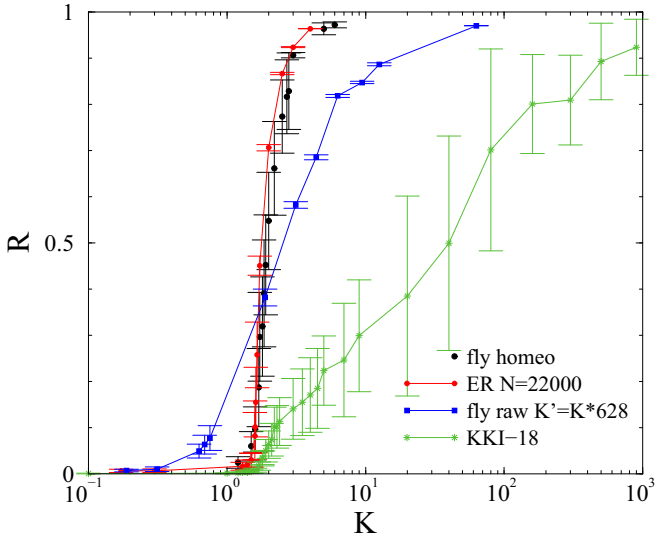

FIG. 3. Synchronization transition of $R(t \to \infty, K)$ on different graphs.

a downward curvature. To see the corrections to scaling we determined the effective exponents of R as the discretized, logarithmic derivative of Eq. (8) at these discrete time steps t_k, near the transition point

$$\eta_{\text{eff}} = \frac{\ln\langle R(t_{k+3})\rangle - \ln\langle R(t_k)\rangle}{\ln(t_{k+3}) - \ln(t_k)}. \tag{11}$$

Here the brackets denote sample averaging over different initial conditions. These effective exponent values can be seen on the local slope inset of the figure. Some fluctuation and modulation effects, coming from the weak modular graph structure of the FF, remain. One can estimate a synchronization transition at $K_c = 1.70(2)$, characterized by $\eta = 0.70(5)$. This is close to the mean-field value, obtained in Refs. [51,62] $\eta_{MF} \simeq 0.75$ and higher than those of the large human white matter connectomes, where the graph dimension was found to be $d < d_c = 4$ [39].

Using the steady-state values we also determined the transition as the function of the control parameter K. Figure 3 displays a comparison of the FF transition with the results obtained on the KKI-18 human connectome. The transition is sharp around $K_c = 1.70(2)$ and R changes from 0.02 to 0.97 as K from 1.2 to 6. In comparison, similar change of R for the KKI-18 spans from $1.6 < K < 10^3$. We also plotted the results obtained without the application of weight normalization by running on the raw FF network on Fig. 3. In this case the transition occurs at a much lower coupling: $K_c = 0.00090(5)$, so we multiplied them on the plot by the average weight value $K' = K \times 628$. Note that the transition of the raw case is not smoother than the homeostatic one, just it appears to be like that, as the consequence of the linear upscaling of K. It happens in the $0.0005 < K < 0.2$ region. The steady-state results on a random ER graph with $N = 22.000$ and $\langle k\rangle = 315$ are also displayed. Here we used weight normalization condition (10) as for FF. The synchronization transition occurs in the $1.4 < K < 5$ region, which is slightly narrower than for the FF.

We can analyze the transition further by determining the fluctuations of $R(t \to \infty, K)$ near the transition. This is plotted on Fig. 4. As we can see the standard deviation: $\sigma(R(t \to \infty, K))$ of the FF is very similar to that of an ER graph of same size and average degree, but somewhat wider. In comparison the KKI-18 exhibits a much more smeared transition region, even though the weighted average degree is smaller: $\langle w\rangle_{\text{KKI}-18} = 448$ than that of the fly connectome: $\langle w\rangle_{\text{FF}} = 628$. As $d_{KKI-18} < d_c^- = 4$ this is a crossover transition and no exact finite scaling is applicable to rescale it.

In case of KM on random ER graphs increasing the size causes small decrease of K_c as well as narrower peaks as

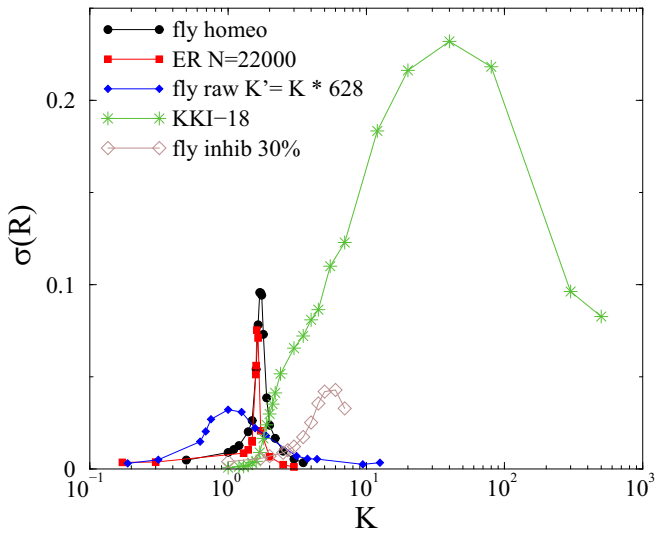

FIG. 4. Fluctuations of $R(t \to \infty, K)$ for different graphs.

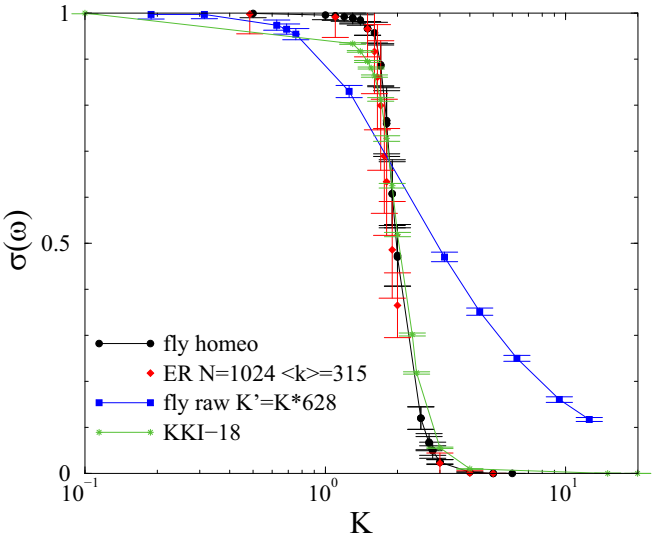

FIG. 5. Frequency entrainment order parameter $\Omega(t \to \infty, K)$ of the KM obtained on different graphs.

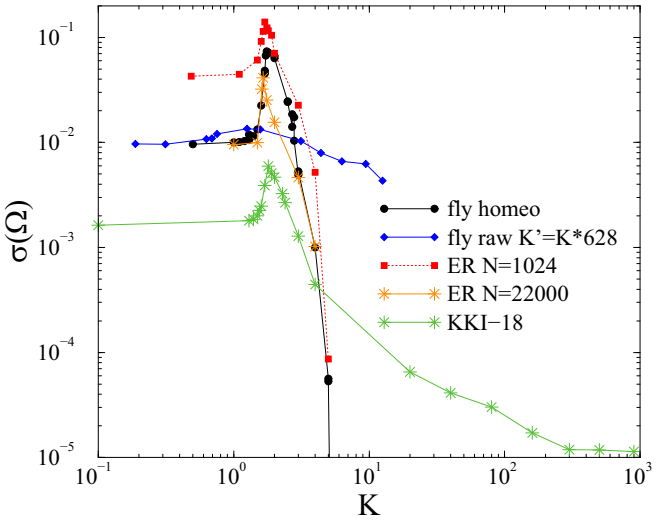

FIG. 6. Fluctuations of the frequency entrainment order parameter $\sigma(\Omega(t \to \infty, K))$ for different graphs.

shown in Ref. [51]. If we increase the average degree from $\langle k \rangle = 4$ to $\langle k \rangle = 350$, the critical point $K_c \simeq 0.482$ moves to $K_c \simeq 1.65$ close to that of the full graph case $K_c \simeq 1.6$. Thus, one may expect that the bigger average degree of FF would cause a peak at larger couplings. In contrast we can see that the hierarchical modular network (HMN) structure of KKI-18 causes nontrivial effects on the $\sigma(R)$ peak and on the width of the phase synchronization transition region.

We have also investigated the frequency synchronization order parameter, which is defined here as Eq. (9). In case of the single peaked Gaussian self-frequencies one can follow the frequency entrainment by this quantity. This has the advantage of having lower critical dimension: $d_c^- = 2$ as compared to the phases: $d_c^- = 4$. This was showed on regular lattices [64], but Ref. [67] obtained similar conclusion on complex network. Thus in case of graph, like the KKI-18, a real frequency phase transition can occur, if we found the human brain to exhibit topological dimension $d > 2$, even for higher resolutions.

Indeed as the Fig. 5 shows the frequency transitions on the fly on the ER and on the human KKI-18 are very similar. Now the finite-size scaling

$$|K - K_c| \propto N^{-1/\tilde{\nu}} \tag{12}$$

is applicable as all of these graphs have $d > d_c^-$. By considering the fluctuations of this order parameter: $\sigma(\Omega(t \to \infty, K))$ we find that the peaks are close, but the KKI-18 transition region is much wider in the high coupling region, than in case of the ER and the FF (see Fig. 6). The fluctuation region on the random ER graph is the narrowest and the peak value decreases as we increase N. We have also plotted the results obtained on the raw FF graph, upscaled by the average value of the weights: $K' = K \times 628$. The distribution looks wider, but this is just the consequence of the horizontal rescaling.

Finally, we also performed measurements for the desynchronization times as in Refs. [51,52]. To define desynchronization avalanches in terms of the Kuramoto order parameter, we can consider processes, starting from fully desynchronized initial states by a single phase perturbation (or by an external phase shift at a node), followed by growth and return to $R(t_x) = 1/\sqrt{N}$, corresponding to the disordered state of N oscillators. In the simulations one can measure the first return, crossing times t_x in many random realizations of the system. In Refs. [51,52], the return or spontaneous desynchronization time was estimated by $t_x = (t_k + t_{k-1})/2$, where t_k was the first measured crossing time, when $R(t_k)$ fell below $1/\sqrt{N}$.

Following a histogramming procedure, one can obtain $p_x(t)$ distributions shown on Fig. 7 for the weight normalized, homeostatic case. For $K = 1.65(5)$ (i.e., near the transition point estimated before), we can find critical PL decay characterized by $\tau_t \simeq 1.6(1)$, close to the mean-field value of the spontaneous desynchronization of $R(t)$, as defined in Ref. [51]. For $K > 1.7$ the curves decay as $p_x(t) \sim 1/t$ up to

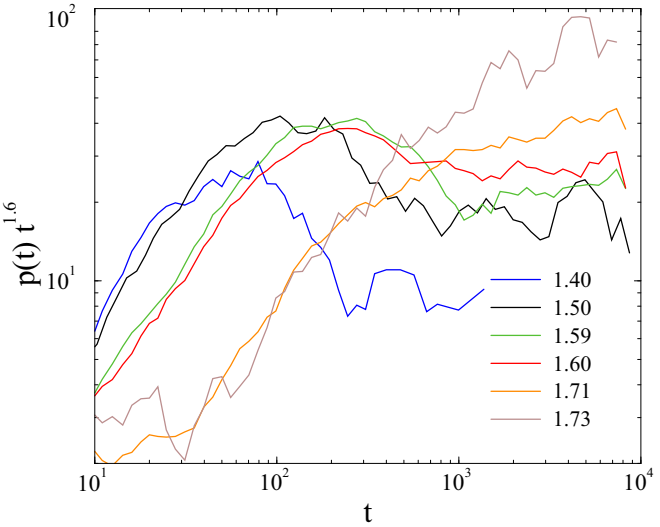

FIG. 7. Desynchronization time distributions $p_x(t)t^{1.6}$ near the transition point in case of the fly connectome with local homeostasis for different couplings, as shown by the legends.

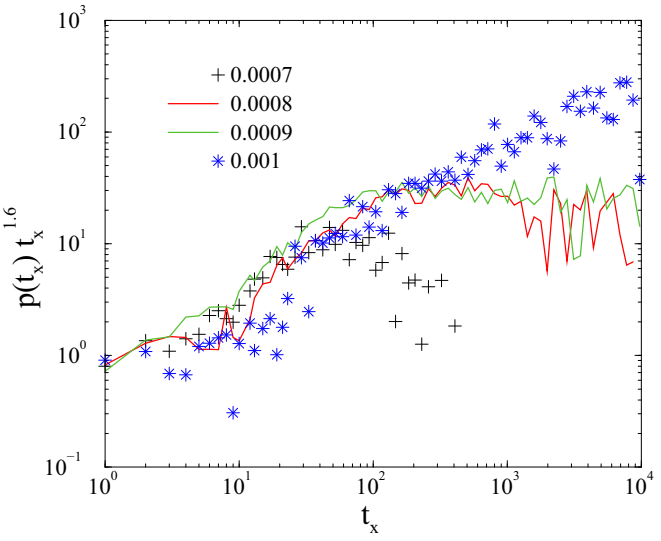

FIG. 8. Desynchronization time distributions $p_x(t)t^{1.6}$ near the transition point, using the raw fly connectome graph for different couplings, as shown by the legends.

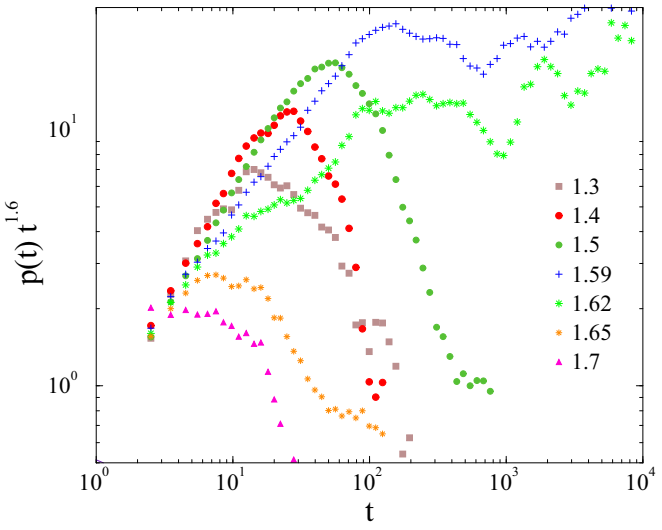

FIG. 9. Desynchronization time distributions $p_x(t)t^{1.6}$ near the transition point in case of ER graphs with different couplings, as shown by the legends.

a cutoff, corresponding to the ordered state, while for $K < 1.5$ the curves break down sharply. It is hard to decide if there is a narrow GP in the $1.5 \leqslant K \leqslant 1.7$ region due to the strong fluctuations remained even after averaging over tens of thousands of samples with different $\omega_{i,0}$ initial conditions.

Similar results have been obtained using the raw FF graph, as shown on Fig. 8. The transition point is at $K_c = 0.0008(1)$, where we can observe a saturation of the $p_x(t)t^{1.6}$ for $t > 200$, thus again mean-field scaling occurs. At $K = 0.001$ we can also see the $p_x(t) \propto 1/t$ decay, corresponding to the synchronized state, in which arbitrarily large decay times can happen, but no signs of subcritical PLs, corresponding to a GP have been found.

For comparison we have done this analysis for full and for ER graphs with $N = 22000$ and $\langle k \rangle = 315$. Now we just show the results for the ER case on Fig. 9. Below $K_c \simeq 1.59$ the $p_x(t)t^{1.6}$ curves break down quickly, without any sign of PL tails. While for $K = 1.59$ we see a saturation for $t > 200$, the $K = 1.62$ curve seems to cross over to the singular $p_x(t) \sim 1/t$ behavior. Going beyond this the curves break down very quickly again, suggesting that within the maximum measurement time $t = 10^4$ desynchronization events could not happen.

We have also tested the effects of the introduction of negative couplings by flipping the sign of outgoing weight values: $W_{ij} = -W_{ij}$ of 30% of randomly chosen nodes. As the consequence the transition region broadens considerably as shown on Fig. 4.

IV. CONCLUSIONS

In conclusion we have investigated KM at the edge of synchronization by comparing the dynamical behavior on the FF, ER, and the KKI-18 large human connectome. The FF network topology is rather similar, almost free of modules, to the high-dimensional ER graph. Thus we found a mean-field-like behavior, unlike for the KKI-18, which has $d < 4$, a HMN structure, which enhances and broadens the transition region with the appearance of GP singularity. Although the link weight distribution of FF exhibits a fat tail, it does not seem to be enough to introduce visible GP effects, or maybe a very weak ones. Thus one can think that the fly brain's simpler structure does not allow the appearance of the complex subcritical dynamical phenomena, which are present in the human brain. The lack of modules on smaller scales may also explain that in global human brain measurements nonuniversal scaling [13] are reported, while local electrode studies [1] show mean-field exponents. Possibly electrode studies [1] measure local activity and within those small volumes modules and GP are less relevant than on the whole brain scale.

The range of the synchronization transition region is slightly broader than in case of the ER, but much narrower than in case of the KKI-18 when we applied link weight normalization, to mimic local homeostasis. This is shown both by the phase and frequency order parameters. Without link weight normalization the KM transition occurs at very low coupling values, but shows mean-field scaling. This was shown by measuring the synchronization growth exponent η and the desynchronization time exponent τ_t.

If we allow negative couplings the transition region broadens further, leading to a spin-glass-like phase, where GP effects may also emerge. But as the details and dynamics of such negative couplings are unknown in case of the FFs we have not investigated this further. We have arrived to similar conclusions as the very recent publication by Buendia *et al.* [68] in case of the complex interplay between structure and dynamics, but we showed the emergence of a critical transition in terms of desynchronization times as well as the initial-slip, characterized by the exponent η.

Given the limitations and assumptions we mentioned in Sec. I, we have provided ample numerical evidence for the different dynamical critical behavior of the Kuramoto model, as the result of the different connectome topology of a fly and of a human brain. Further studies on other animals, preferably

mammals, should be performed in order to fully justify the proposition expressed in the title.

ACKNOWLEDGMENTS

We thank Róbert Juhász and Shengfeng Deng for useful comments and discussions. G.Ó. is supported by the National Research, Development and Innovation Office NKFIH under Grant No. K128989 and the Project HPC-EUROPA3 (INFRAIA-2016-1-730897) from the EC Research Innovation Action under the H2020 Programme. We thank access to the Hungarian national supercomputer network NIIF and to BSC Barcelona. G.D. is supported by the project PID2019-105772GB-I00/AEI/10.13039/501100011033 financed by the Ministry of Science, Innovation and Universities (MCIU) and the State Research Agency (AEI)10.

[1] J. Beggs and D. Plenz, Neuronal avalanches in neocortical circuits, J. Neuroscience **23**, 11167 (2003).
[2] A. Mazzoni, F. D. Broccard, E. Garcia-Perez, P. Bonifazi, M. E. Ruaro, and V. Torre, On the dynamics of the spontaneous activity in neuronal networks, PLoS One **2**, e439 (2007).
[3] V. Pasquale, P. Massobrio, L. L. Bologna, M. Chiappalone, and S. Martinoia, Self-organization and neuronal avalanches in networks of dissociated cortical neurons, Neuroscience **153**, 1354 (2008).
[4] N. Friedman, S. Ito, B. A. W. Brinkman, M. Shimono, R. E. L. DeVille, K. A. Dahmen, J. M. Beggs, and T. C. Butler, Universal Critical Dynamics in High Resolution Neuronal Avalanche Data, Phys. Rev. Lett. **108**, 208102 (2012).
[5] G. Hahn, T. Petermann, M. N. Havenith, S. Yu, W. Singer, D. Plenz, and D. Nikolić, Neuronal avalanches in spontaneous activity in vivo, J. Neurophysiol. **104**, 3312 (2010).
[6] O. Shriki, J. Alstott, F. Carver, T. Holroyd, R. N. A. Henson, M. L. Smith, R. Coppola, E. Bullmore, and D. Plenz, Neuronal avalanches in the resting meg of the human brain, J. Neurosci. **33**, 7079 (2013).
[7] E. Tagliazucchi, P. Balenzuela, D. Fraiman, and D. Chialvo, Criticality in large-scale brain fmri dynamics unveiled by a novel point process analysis, Front. Physiol. **3**, 15 (2012).
[8] G. Scott, E. D. Fagerholm, H. Mutoh, R. Leech, D. J. Sharp, W. L. Shew, and T. Knöpfel, Voltage imaging of waking mouse cortex reveals emergence of critical neuronal dynamics, J. Neurosci. **34**, 16611 (2014).
[9] V. Priesemann, M. Wibral, M. Valderrama, R. Pröpper, M. Le Van Quyen, T. Geisel, J. Triesch, D. Nikolić, and M. H. J. Munk, Spike avalanches in vivo suggest a driven, slightly subcritical brain state, Front. Syst. Neurosci. **8**, 108 (2014).
[10] T. Bellay, A. Klaus, S. Seshadri, and D. Plenz, Irregular spiking of pyramidal neurons organizes as scale-invariant neuronal avalanches in the awake state, Elife **4**, e07224 (2015).
[11] G. Hahn, A. Ponce-Alvarez, C. Monier, G. Benvenuti, A. Kumar, F. Chavane, G. Deco, and Y. Frégnac, Spontaneous cortical activity is transiently poised close to criticality, PLoS Comput. Biol. **13**, e1005543 (2017).
[12] S. Seshadri, A. Klaus, D. Winkowski *et al.*, Altered avalanche dynamics in a developmental nmdar hypofunction model of cognitive impairment, Transl Psychiatry **8**, 3(2018).
[13] J. M. Palva, A. Zhigalov, J. Hirvonen, O. Korhonen, K. Linkenkaer-Hansen, and S. Palva, Neuronal long-range temporal correlations and avalanche dynamics are correlated with behavioral scaling laws, Proc. Nat. Acad. Sci. USA **110**, 3585 (2013).
[14] D. R. Chialvo and P. Bak, Learning from mistakes, Neuroscience **90**, 1137 (1999).
[15] D. R. Chialvo, Critical brain networks, Physica A **340**, 756 (2004), complexity and Criticality: in memory of Per Bak (1947–2002).
[16] D. R. Chialvo, Are our senses critical? Nature Phys. **2**, 301 (2006).
[17] D. R. Chialvo, The brain near the edge, in *Cooperative Behavior in Neutral Systems: Ninth Granada Lectures*, edited by J. Marro, P. L. Garrido, and J. J. Torres, AIP Conf. Proc. No. 887 (AIP, New York, 2007), p. 1.
[18] D. R. Chialvo, P. Balenzuela, and D. Fraiman, The brain: What is critical about it? in *Collective Dynamics: Topics on Competition and Cooperation in the Bioscience: A Selection of Papers in the Proceedings of the BIOCOMP2007 International Conference*, edited by L. M. Ricciardi, A. Buonocore, and E.Pirozzi, AIP Conf. Proc. No. 1028 (AIP, New York, 2008), p. 28.
[19] D. Fraiman, P. Balenzuela, J. Foss, and D. R. Chialvo, Ising-like dynamics in large-scale functional brain networks, Phys. Rev. E **79**, 061922 (2009).
[20] P. Expert, R. Lambiotte, D. R. Chialvo, K. Christensen, H. J. Jensen, D. J. Sharp, and F. Turkheimer, Self-similar correlation function in brain resting-state functional magnetic resonance imaging, J. R. Soc. Interface **8**, 472 (2011).
[21] D. Fraiman and D. Chialvo, What kind of noise is brain noise: anomalous scaling behavior of the resting brain activity fluctuations, Front. Physiol. **3**, 307 (2012).
[22] G. Deco and V. K. Jirsa, Ongoing cortical activity at rest: Criticality, multistability, and ghost attractors, J. Neurosci. **32**, 3366 (2012).
[23] G. Deco, A. Ponce-Alvarez, P. Hagmann, G. L. Romani, D. Mantini, and M. Corbetta, How local excitation-inhibition ratio impacts the whole brain dynamics, J. Neurosci. **34**, 7886 (2014).
[24] M. Senden, N. Reuter, M. P. van den Heuvel, R. Goebel, and G. Deco, Cortical rich club regions can organize state-dependent functional network formation by engaging in oscillatory behavior, NeuroImage **146**, 561 (2017).
[25] M. A. Muñoz, Colloquium: Criticality and dynamical scaling in living systems, Rev. Mod. Phys. **90**, 031001 (2018).
[26] A. Haimovici, E. Tagliazucchi, P. Balenzuela, and D. R. Chialvo, Brain Organization into Resting State Networks Emerges at Criticality on a Model of the Human Connectome, Phys. Rev. Lett. **110**, 178101 (2013).
[27] J. J. Johnson S., Torres and J. Marro, Robust short-term memory without synaptic learning, PLoS One **8**, e50276 (2013).
[28] P. Bak, C. Tang, and K. Wiesenfeld, Self-organized criticality: An explanation of the $1/f$ noise, Phys. Rev. Lett. **59**, 381 (1987).
[29] D. R. Chialvo, Emergent complex neural dynamics, Nature Phys. **6**, 744 (2010).

[30] J. Touboul and A. Destexhe, Power-law statistics and universal scaling in the absence of criticality, Phys. Rev. E **95**, 012413 (2017).

[31] T. Vojta, Rare region effects at classical, quantum and nonequilibrium phase transitions, J. Phys. A: Math. Gen. **39**, R143 (2006).

[32] R. B. Griffiths, Nonanalytic Behavior Above the Critical Point in a Random Ising Ferromagnet, Phys. Rev. Lett. **23**, 17 (1969).

[33] G. Ódor, Slow, bursty dynamics as a consequence of quenched network topologies, Phys. Rev. E **89**, 042102 (2014).

[34] M. Karsai, H.-H. Jo, and K. Kaski, Bursty human dynamics, SpringerBriefs in Complexity (2018).

[35] W. Cota, S. C. Ferreira, and G. Ódor, Griffiths effects of the susceptible-infected-susceptible epidemic model on random power-law networks, Phys. Rev. E **93**, 032322 (2016).

[36] M. A. Muñoz, R. Juhász, C. Castellano, and G. Ódor, Griffiths Phases on Complex Networks, Phys. Rev. Lett. **105**, 128701 (2010).

[37] G. Ódor, R. Dickman, and G. Ódor, Griffiths phases and localization in hierarchical modular networks, Sci. Rep. **5**, 14451 (2015).

[38] W. Cota, G. Ódor, and S. C. Ferreira, Griffiths phases in infinite-dimensional, non-hierarchical modular networks, Sci. Rep. **8**, 9144 (2018).

[39] M. T. Gastner and G. Ódor, The topology of large Open Connectome networks for the human brain, Sci. Rep. **6**, 27249 (2016).

[40] G. Ódor, Critical dynamics on a large human open connectome network, Phys. Rev. E **94**, 062411 (2016).

[41] G. Ódor, M. T. Gastner, J. Kelling, and G. Deco, Modelling on the very large-scale connectome, J. Phys. Complex. **2**, 045002 (2021).

[42] O. Sporns, G. Tononi, and R. Kötter, The Human Connectome: A Structural Description of the Human Brain, PLoS Comput. Biol. **1**, e42 (2005).

[43] L. K. Scheffer and I. A. Meinertzhagen, The fly brain atlas, Annu. Rev. Cell Dev. Biol. **35**, 637 (2019).

[44] C. S. Xu, M. Januszewski, Z. Lu, Shin-ya Takemura, K. J. Hayworth, G. Huang, K. Shinomiya, J. Maitin-Shepard, D. Ackerman, S. Berg, T. Blakely, J. Bogovic, J. Clements, T. Dolafi, P. Hubbard, D. Kainmueller, W. Katz, T. Kawase, K. A. Khairy, L. Leavitt *et al.*, *A Connectome of the Adult Drosophila Central Brain* (Cold Spring Harbor Laboratory, 2020).

[45] Y. Penn, M. Segal, and E. Moses, Network synchronization in hippocampal neurons, Proc. Nat. Acad. Sci. USA **113**, 3341 (2016).

[46] S. di Santo, P. Villegas, R. Burioni, and M. A. Muñoz, Landau–ginzburg theory of cortex dynamics: Scale-free avalanches emerge at the edge of synchronization, Proc. Nat. Acad. Sci. USA **115**, E1356 (2018).

[47] Y. Kuramoto, *Chemical Oscillations, Waves, and Turbulence*, Springer Series in Synergetics (Springer, Berlin, 2012)

[48] P. Villegas, P. Moretti, and M. A. Muñoz, Frustrated hierarchical synchronization and emergent complexity in the human connectome network, Sci. Rep. **4**, 5990 (2014).

[49] P. Villegas, J. Hidalgo, P. Moretti, and M. A. Muñoz, Complex synchronization patterns in the human connectome network, *Proceedings of ECCS 2014 European Conference on Complex Systems* (Springer, 2016), pp. 69–80.

[50] A. P. Millán, J. J. Torres, and G. Bianconi, Complex network geometry and frustrated synchronization, Sci. Rep. **8**, 9910 (2018).

[51] G. Ódor and J. Kelling, Critical synchronization dynamics of the kuramoto model on connectome and small world graphs, Sci. Rep. **9**, 19621 (2019).

[52] G. Ódor, J. Kelling, and G. Deco, The effect of noise on the synchronization dynamics of the kuramoto model on a large human connectome graph, Neurocomputing **461**, 696 (2021).

[53] C. Delettre, A. Messé, L.-A. Dell, O. Foubet, K. Heuer, B. Larrat, S. Meriaux, J.-F. Mangin, I. Reillo, C. de Juan Romero, V. Borrell, R. Toro, and C. C. Hilgetag, Comparison between diffusion MRI tractography and histological tract-tracing of cortico-cortical structural connectivity in the ferret brain, Network Neuroscience **3**, 1038 (2019).

[54] D. M. Abrams and S. H. Strogatz, Chimera States for Coupled Oscillators, Phys. Rev. Lett. **93**, 174102 (2004).

[55] L. J. Fosque, R. V. Williams-García, J. M. Beggs, and G. Ortiz, Evidence for Quasicritical Brain Dynamics, Phys. Rev. Lett. **126**, 098101 (2021).

[56] The hemibrain dataset (v1.0.1), 2020.

[57] L. K. Scheffer, Graph properties of the adult Drosophila central brain, bioRxiv (2020), doi: 10.1101/2020.05.18.102061.

[58] D. J. Watts and S. H. Strogatz, Collective dynamics of small-world networks, Nature (London) **393**, 440 (1998).

[59] A. Fronczak, P. Fronczak, and J. A. Hołyst, Average path length in random networks, Phys. Rev. E **70**, 056110 (2004).

[60] M. D. Humphries and K. Gurney, Network 'Small-World-Ness': A Quantitative Method for Determining Canonical Network Equivalence, PLoS One **3**, e0002051 (2008).

[61] H. Hong, H. Chaté, H. Park, and L.-H. Tang, Entrainment transition in populations of random frequency oscillators, Phys. Rev. Lett. **99**, 184101 (2007).

[62] C. Choi, M. Ha, and B. Kahng, Extended finite-size scaling of synchronized coupled oscillators, Phys. Rev. E **88**, 032126 (2013).

[63] R. Juhász, J. Kelling, and G. Ódor, Critical dynamics of the Kuramoto model on sparse random networks, J. Stat. Mech.: Theory Exp. **2019**, 053403 (2019).

[64] H. Hong, H. Park, and M. Y. Choi, Collective synchronization in spatially extended systems of coupled oscillators with random frequencies, Phys. Rev. E **72**, 036217 (2005).

[65] D. P., Order and stepsize control in extrapolation methods, Numer. Math. **41**, 399 (1983).

[66] R. P. Rocha, L. Koçillari, S. Suweis, M. Corbetta, and A. Maritan, Homeostatic plasticity and emergence of functional networks in a whole-brain model at criticality, Sci. Rep. **8** (2018).

[67] A. P. Millán, J. J. Torres, and G. Bianconi, Synchronization in network geometries with finite spectral dimension, Phys. Rev. E **99**, 022307 (2019).

[68] V. Buendia, P. Villegas, R. Burioni, and M. A. Munoz, The broad edge of synchronisation: Griffiths effects and collective phenomena in brain networks, arXiv:2109.11783 [Philos. Trans. Royal Soc. A (to be published)].